Int. J. Heat Mass Transfer. Vol. 33, No. 5, pp. 847–857, 1990
Printed in Great Britain

0017–9310/90 $3.00 + 0.00

Transient characteristics of combined conduction, convection and radiation heat transfer in porous media

H. YOSHIDA, J. H. YUN and R. ECHIGO
Department of Mechanical Engineering, Tokyo Institute of Technology, Tokyo 152, Japan

and

T. TOMIMURA
Institute of Advanced Material Study, Kyushu University, Kasuga 816, Japan

(*Received* 10 *May* 1989 *and in final form* 13 *July* 1989)

Abstract—This paper presents transient heat transfer characteristics of an effective energy conversion between high-temperature gas enthalpy and thermal radiation by means of porous media. A theoretical analysis is conducted for the one-dimensional system where conduction, convection and radiation take place simultaneously. The porous medium is assumed to be a homogeneous continuum which absorbs and emits thermal radiation. The coupled energy equations for gas and porous media are solved numerically. To confirm the validity of the analysis, experiments which strictly correspond to the analytical model are performed. The predicted results agree well with those of the experiments.

1. INTRODUCTION

IN HIGH-temperature systems, a key to the heat transfer enhancement is the effective use of thermal radiation which becomes increasingly efficient as the system temperature increases. The emissive power of gas, however, is so small that a 'radiative converter', which converts the energy of high-temperature gas into thermal radiation, is necessary.

One of the authors analyzed a heat transfer system where high-temperature gas passes through a porous medium placed in a duct, and showed that the porous medium can effectively convert the gas enthalpy into thermal radiation [1]. This conversion consists of two heat transfer processes: one is the convection between gas and porous media due to the high heat transfer coefficient and the large surface area; the other is the radiation from the porous medium the emissive power of which is much higher than that of gases. The most outstanding feature of the phenomenon is that thermal radiation emitted from the porous medium propagates chiefly in the upstream direction. Owing to the strong directionality of this radiative converter, it has been applied to various industrial furnaces, and has attained remarkable energy-saving and combustion enhancement [2–8].

Although the original theoretical analysis [1] clarified the basic heat transfer characteristics of the radiative converter, there are still many important aspects which have not been discussed yet. The essential assumptions introduced in the previous analysis are: the system is one-dimensional and steady; the working gas is nonradiating; and scattering in the porous medium is negligible. Since these assumptions are not always valid in a variety of applications, theoretical studies complementary to the original work have also been required. Of these, Wang and Tien [9] investigated the effect of scattering in the porous medium, while Echigo *et al.* [10] studied the effect of gaseous radiation which is not always small if radiating gases such as carbon dioxide or steam are contained in the working fluid.

The purpose of this study is to examine the transient heat transfer response relevant to actual operations of the radiative converter.† This problem also serves as a benchmark to develop an accurate analytical model, because the system undergoes a rapid change with a large temperature difference. Accuracy of the analytical model and numerical code is confirmed in terms of the comparison with actual experimentation of the method.

2. ANALYSIS

2.1. *Analytical model and governing equations*

A schematic diagram of the physical system is shown in Fig. 1. A porous medium (geometric thickness x_p, optical thickness τ_p, and porosity ψ) is placed normal to a gas flow, and the flow and heat transfer are one-dimensional. Initially (for time $t < 0$), the gas and porous medium are at room temperature θ_0

† The present study is closely connected to the heat transfer characteristics of the regenerator used in Stirling engines.

NOMENCLATURE

- c specific heat [J kg^{-1} K^{-1}]
- E_1, E_2, E_3 exponential integrals
- h heat transfer coefficient [W m^{-2} K^{-1}]
- L length scale ratio, sx_p^2/l
- l characteristic length of a porous medium [m]
- n number of nodal points in a porous region
- N_l dimensionless parameter, $Nu\,L$
- N_r conduction–radiation parameter, $\lambda_g\kappa/(\sigma\theta_1^3)$
- Nu Nusselt number, hl/λ_g
- Pe Peclet number, $\rho_g c_g u x_p/\lambda_g$
- q radiative heat flux [W m^{-2}]
- r incident radiative heat flux [W m^{-2}]
- s surface area per unit volume of a porous medium [m^2 m^{-3}]
- t time [s]
- u gas velocity [m s^{-1}]
- x coordinate [m]
- x_p thickness of a porous medium [m].

Greek symbols

- Γ heat capacity ratio, $\rho_p c_p/(\rho_g c_g)$
- θ temperature [K]
- θ_0 initial gas temperature [K]
- θ_1 steady-state gas temperature [K]
- κ absorption coefficient [m^{-1}]
- λ thermal conductivity [W m^{-1} K^{-1}]
- ρ (bulk) density [kg m^{-3}]
- σ Stefan–Boltzmann coefficient, 5.67×10^{-8} [W m^{-2} K^{-4}]
- τ optical depth
- τ_p optical thickness of a porous medium
- ψ porosity of a porous medium.

Subscripts

- d downstream
- g gas
- p porous medium
- n net
- u upstream
- I upstream boundary
- II entrance of a porous medium
- III exit of a porous medium
- IV downstream boundary.

Superscripts

- + forward direction
- − backward direction.

throughout. While the gas steadily passes through the porous medium with velocity u, its temperature θ_g is suddenly raised to θ_1 at time $t = 0$. Simultaneously, incident radiations $r_u = \sigma\theta_u^4$ and $r_d = \sigma\theta_d^4$ from the upstream and downstream sides, respectively, are applied to the system.

To obtain the basic equations for the system, the following assumptions are introduced.

(1) The porous medium is a homogeneous continuum the thermophysical properties of which are given by multiplying those of the porous material by a factor of $(1-\psi)$.

(2) In practice, however, the factor $(1-\psi)$ is important only to evaluate the bulk density of the porous medium ρ_p which is included in the unsteady term of the energy equation. This is based on the fact that the porosity ψ of the porous medium dealt with here is close to unity, and thus $(1-\psi)$ is nearly equal to zero. Accordingly, the effective thermal conductivity of the porous medium is negligible.

(3) Owing to the high porosity mentioned above, the gas flow is free from the blockage effect of the porous medium. Hence, the interaction between gas and porous media appears only in the heat transfer term in the energy equations.

(4) All the thermophysical properties are constant.

In addition to these assumptions, we consider the case for a non-radiating gas and a non-scattering medium. Thus, the optical depth and thickness of the porous medium are given by $\tau = \kappa x$ and $\tau_p = \kappa x_p$, respectively, where κ is the absorption coefficient. On the basis of the previous analysis conducted by Echigo [1], we can obtain the following governing equations for transient heat transfer.

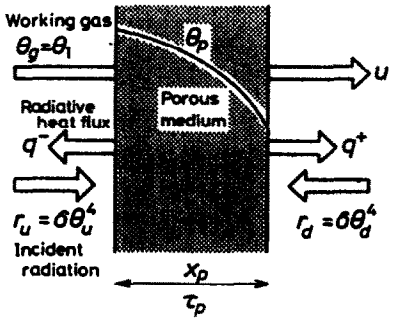

FIG. 1. Schematic diagram of the physical system.

Energy equation for gas

$$\rho_g c_g \frac{\partial\theta_g}{\partial t} = -\rho_g c_g u \frac{\partial\theta_g}{\partial x} + \lambda_g \frac{\partial^2\theta_g}{\partial x^2} - hs(\theta_g - \theta_p). \quad (1)$$

Energy equation for porous medium

$$\rho_p c_p \frac{\partial\theta_p}{\partial t} = -\frac{\partial q_n}{\partial x} - hs(\theta_p - \theta_g). \quad (2)$$

It should be noted in equation (1) that the heat con-

duction term, which was neglected in the previous analysis for steady state, is taken into account in the present case. The necessity of this term is described later in connection with the boundary conditions. The last terms on the right-hand sides of equations (1) and (2) express the heat transfer between the gas and the porous medium, where h and s are its coefficient and surface area per unit volume (specific surface area), respectively. The net radiative heat flux q_n appearing in equation (2) is written in terms of the heat flux in the forward and backward directions as

$$q_n = q^+ - q^- \tag{3}$$

$$q^+(\tau) = 2\left[r_u E_3(\tau) + \int_0^\tau \sigma\theta_p(\tau')^4 E_2(\tau-\tau')\,d\tau'\right] \tag{4}$$

$$q^-(\tau) = 2\left[r_d E_3(\tau_p-\tau) + \int_\tau^{\tau_p} \sigma\theta_p(\tau')^4 E_2(\tau'-\tau)\,d\tau'\right] \tag{5}$$

where E_2 and E_3 are the exponential integrals given by

$$E_j(\tau) = \int_0^1 \mu^{j-2}\exp(-\tau/\mu)\,d\mu. \tag{6}$$

Using the recurrence relation for the exponential integrals

$$\frac{d}{d\tau}E_j(\tau) = -E_{j-1}(\tau) \quad (j \geqslant 2) \tag{7}$$

the divergence of net radiative heat flux is expressed as

$$\frac{1}{\kappa}\frac{\partial q_n(x)}{\partial x} = \frac{\partial q_n(\tau)}{\partial \tau} = 2\left[-r_u E_2(\tau) - r_d E_2(\tau_p-\tau) + 2\sigma\theta_p^4 - \int_0^\tau \sigma\theta_p(\tau')^4 E_1(\tau-\tau')\,d\tau' - \int_\tau^{\tau_p} \sigma\theta_p(\tau')^4 E_1(\tau'-\tau)\,d\tau'\right]. \tag{8}$$

Since the radiative heat flux (or its divergence) can be expressed as a function of the porous medium temperature θ_p, equations (1) and (2) constitute the coupled integro-differential equations for the unknowns of θ_g and θ_p.

Dimensionless variables and parameters are introduced as follows:

$$T = \sigma\theta_1^3 t/(\rho_p c_p x_p), \quad X = x/x_p$$

$$\Theta_g = \theta_g/\theta_1, \quad \Theta_p = \theta_p/\theta_1$$

$$Q_n = q_n/(\sigma\theta_1^4), \quad Q^+ = q^+/(\sigma\theta_1^4), \quad Q^- = q^-/(\sigma\theta_1^4)$$

$$R_u = r_u/(\sigma\theta_1^4) = (\theta_u/\theta_1)^4 = \Theta_u^4$$

$$R_d = r_d/(\sigma\theta_1^4) = (\theta_d/\theta_1)^4 = \Theta_d^4$$

$$Pe = \rho_g c_g u x_p/\lambda_g$$

$$Nu = hl/\lambda_g, \quad L = sx_p^2/l, \quad N_l = Nu\,L$$

$$N_r = \lambda_g\kappa/(\sigma\theta_1^3), \quad \Gamma = \rho_p c_p/(\rho_g c_g) \tag{9}$$

where Pe is the Peclet number, Nu the Nusselt number, l the characteristic length of the porous medium (here, the diameter of fine wires), L the length scale ratio, N_r the conduction–radiation parameter, and Γ the thermal capacitance ratio. Using these dimensionless variables and parameters, the governing equations (1)–(5), and (8) are normalized as follows:

$$\frac{\partial\Theta_g}{\partial T} = \frac{N_r\Gamma}{\tau_p}\left[-Pe\frac{\partial\Theta_g}{\partial X} + \frac{\partial^2\Theta_g}{\partial X^2} - N_l(\Theta_g-\Theta_p)\right] \tag{10}$$

$$\frac{\partial\Theta_p}{\partial T} = -\tau_p\frac{\partial Q_n}{\partial\tau} - \frac{N_r N_l}{\tau_p}(\Theta_p-\Theta_g) \tag{11}$$

$$Q_n = Q^+ - Q^- \tag{12}$$

$$Q^+(\tau) = 2\left[R_u E_3(\tau) + \int_0^\tau \Theta_p(\tau')^4 E_2(\tau-\tau')\,d\tau'\right] \tag{13}$$

$$Q^-(\tau) = 2\left[R_d E_3(\tau_p-\tau) + \int_\tau^{\tau_p} \Theta_p(\tau')^4 E_2(\tau'-\tau)\,d\tau'\right] \tag{14}$$

$$\frac{\partial Q_n(\tau)}{\partial\tau} = 2\left[-R_u E_2(\tau) - R_d E_2(\tau_p-\tau) + 2\Theta_p^4 - \int_0^\tau \Theta_p(\tau')^4 E_1(\tau-\tau')\,d\tau' - \int_\tau^{\tau_p} \Theta_p(\tau')^4 E_1(\tau'-\tau)\,d\tau'\right]. \tag{15}$$

In the present analysis, the Reynolds number does not appear explicitly in the governing equations. However, its effect is included implicitly in the Nusselt number, Nu. That is, the heat transfer coefficient between the gas and porous medium is evaluated by assuming that the porous medium consists of fine wires (cylinders), and using the empirical correlation for a cylinder in cross flow [11]. Thus, Nu is given as a function of the Reynolds number.

2.2. *Boundary and initial conditions*

Equations (10) and (11) are to be solved by prescribing appropriate boundary and initial conditions. In the previous analysis, not taking into account the gas-phase conduction [1], the boundary condition for the gas temperature is given at the upstream end of the porous medium; namely, $\Theta_g = \Theta_1$ at $X = X_{II}$ (see

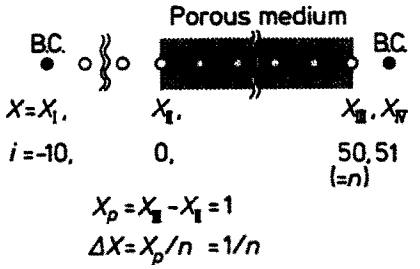

FIG. 2. Computational domain and nodal points.

Fig. 2). This boundary condition is reasonable for the steady state where the porous medium temperature Θ_p at $X = X_{II}$ is also high (and, of course, the Peclet number Pe is not very small). In the initial period of transient heat transfer, however, the porous medium temperature Θ_p at $X = X_{II}$ is so low that the gas temperature Θ_g at $X = 0$ also decreases. As a result, there exists a large gradient of the gas temperature in the region immediately upstream from the porous medium. To predict such phenomena appropriately, the heat conduction term is included and the computational domain is extended over the region upstream of the porous medium as well as the porous region (Fig. 2). Hence, the boundary conditions are given as follows:

$$X = X_I: \quad \Theta_g = \Theta_I \tag{16}$$

$$X = X_{IV}: \quad \partial\Theta_g/\partial X = 0. \tag{17}$$

The calculated results with and without the gas-phase conduction are compared in Appendix A. On the other hand, the initial condition is

$$T < 0: \quad \Theta_g = \Theta_p = \Theta_0. \tag{18}$$

2.3. *Numerical procedures*

The transient energy equations (10) and (11) were solved by numerical means. We used an implicit scheme based on the two-level time discretization, which is analogous to the Crank–Nicolson method. It should be noted here that the types of equations, equations (10) and (11), differ a great deal from each other; the former is a parabolic partial differential equation, while the latter is a non-linear integro-differential equation without the second derivative.

As shown in Fig. 2, a uniform grid of 62 nodal points was used (i.e. $i = -10 \sim -1$ for the upstream region; $i = 0 \sim 50$ for the porous region; $i = 51$ for the downstream regions). The solution procedure for each nodal point is as follows.

$i = -9 \sim -1$. Since the porous medium does not exist in the region, only equation (10) is solved, omitting the heat transfer term.

$i = 0$. In the control volume of $-\Delta X/2 \leqslant X \leqslant \Delta X/2$, there exists a porous medium on the positive side ($0 \leqslant X \leqslant \Delta X/2$), whereas it does not exist on the negative side ($-\Delta X/2 \leqslant X \leqslant 0$). Hence, by integrating the equations over the control volume, we obtain the energy balance in the volume, and solve the equations for Θ_g and Θ_p.

$i = 1 \sim 49$. Equations (10) and (11) are directly solved according to the usual finite difference scheme (without the integration of equations as explained at $i = 0$).

$i = 50$. Since the situation is similar to that for $i = 0$, we solve the equations for Θ_g and Θ_p, noting the boundary condition at $X = X_{IV}$.

Owing to the neglection of scattering, the equations can be solved rigorously. The numerical integrations of the radiative heat flux and its divergence are carried out using the trapezoidal rule. Results are expressed in terms of the summation of matrices which consist of the exponential integrals. The terms including Θ_p in equations (13)–(15) are calculated as follows (the detailed derivation and the nomenclature are shown in Appendix B):

$$\int_0^{\tau_i} \Theta_p(\tau')^4 E_2(\tau_i - \tau')\,d\tau' = \sum_{j=0}^{i} [\Theta_{pj}^4 \mathrm{E3MATP}(i,j)] \tag{19}$$

$$\int_{\tau_i}^{\tau_p} \Theta_p(\tau')^4 E_2(\tau' - \tau_i)\,d\tau' = \sum_{j=i}^{n} [\Theta_{pj}^4 \mathrm{E3MATN}(i,j)] \tag{20}$$

$$2\Theta_p(\tau_i)^4 - \int_0^{\tau} \Theta_p(\tau')^4 E_1(\tau - \tau')\,d\tau' - \int_{\tau}^{\tau_p} \Theta_p(\tau')^4 E_1(\tau' - \tau)\,d\tau' = \sum_{j=0}^{n} [\Theta_{pj}^4 \mathrm{E2MAT}(i,j)]. \tag{21}$$

Here, the exponential integrals E_2 and E_1 are transformed to E_3 and E_2, respectively, using the recurrence relation. The energy balance obtained from the calculated results is satisfied within the accuracy of about 1%.

3. EXPERIMENT

Experiments were performed in order to confirm the validity of the analysis. For this purpose, the apparatus was designed to correspond exactly to the analytical model. The points on which special attention was paid were:

(1) one-dimensionality of flow and heat transfer;
(2) ability to independently set gas temperature and incident radiation temperature;
(3) step change of the gas temperature.

In addition to these points, the choice of a working gas was also crucial. Provided that combustion gas is used as the working gas, condensation and evap-

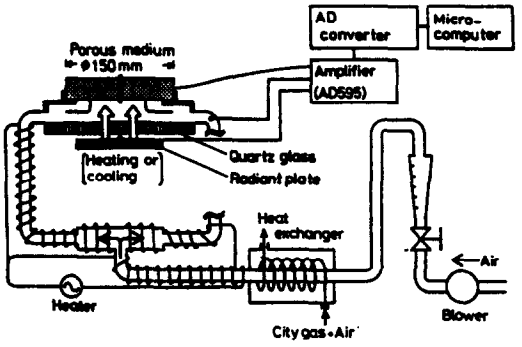

FIG. 3. Schematic outline of the experimental apparatus.

oration of H_2O contained in it complicate the heat transfer phenomena. Hence, we used hot air as the high-temperature working gas instead of combustion gas. This choice has another merit that the air is virtually a non-radiating fluid.

3.1. *Apparatus*

The schematic outline of the apparatus is shown in Fig. 3, and details of the test section are shown in Fig. 4. The air was heated to about 1000 K by a heat exchanger with a combustion load of 100 kW. Six air inlets were installed around the test section; the piping between the heat exchanger and the inlets was subheated to prevent the air from cooling. The temperature of incident radiation was set independently from that of the working gas; a radiant plate was installed upstream of a quartz glass, and its temperature was controlled via an electric heater or cooling water. The radiant plate (stainless steel) was oxidized so that its emissivity was approximately unity. The diameter of the porous medium was 150 mm, and the spacing between the porous medium and radiant plate was 24 mm, which gave the configuration factor of 0.73. Although this factor is somewhat smaller than unity, a one-dimensionality of radiative heat transfer was considered to be sufficient because the test section was insulated. To achieve the step change in the gas temperature, an alternative method was adopted; that is, the porous medium was designed so that it could be mounted instantaneously on the experimental apparatus.

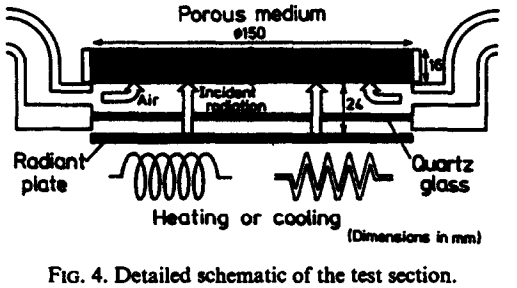

FIG. 4. Detailed schematic of the test section.

3.2. *Porous medium*

The porous medium used in the present experiment consisted of stacks of 40 stainless-steel wire mesh screens of nominal mesh length 1/50 in.; the thickness x_p was 16 mm, and the absorption coefficient κ was 1.25×10^3 m^{-1}. The absorption coefficient was obtained by measuring the amount of attenuation of a laser beam in traveling through the porous medium. Since the scattering was negligible in the present porous medium, the optical thickness was given by $\tau_p = \kappa x_p = 20$. The temperature of the porous medium was measured by six chromel–alumel thermocouples inserted between mesh screens. Since the diameter of the thermocouples was the same as that of the mesh screens, the measured temperature was regarded as the porous medium temperature. The amplified output of the thermocouples was processed by an on-line microcomputer system.

3.3. *Procedure*

Prior to the transient heat transfer experiment, it is necessary for the experimental system, except the porous medium, to reach a steady-state thermal condition ($\theta = \theta_i$). For this, a temporary porous medium was first installed in place of the measuring porous medium. After the system reached the steady-state condition, the temporary porous medium was replaced instantaneously with the measuring porous medium. Since this condition was carried out manually, the time uncertainty associated with the operation was about 1 s, which was negligible compared to the time constant of the phenomena. As the principal parameters of the experiment, the gas velocity u and the incident radiation temperature from the upstream side θ_u were varied systematically. The temperature of the high-temperature working gas θ_i was constant (about 1000 K).

In addition to the experiments described above, we also made a 'cooling' experiment. In the cooling experiment, the porous medium, which had already reached the steady state for the high-temperature working gas ($\theta_g = \theta_i$), was cooled by the low-temperature gas ($\theta_g = \theta_0$). To perform the cooling experiment we prepared an apparatus which was similar to that shown in Fig. 3 but without heating equipment for the working gas.

4. RESULTS AND DISCUSSION

4.1. *Outline of measured temperature history*

Prior to the comparison between analytical and experimental results, we show a typical example of the measured temperature variations. In Fig. 5 the variations of the porous medium temperature θ_p are displayed for three gas velocities. The temperature rise at the entrance of the porous medium (denoted by #1) is much quicker than that observed at the exit (denoted by #6). Although the time constant for the whole system increases with decreasing gas velocity u, it is merely an order of 100 s even in the case of the

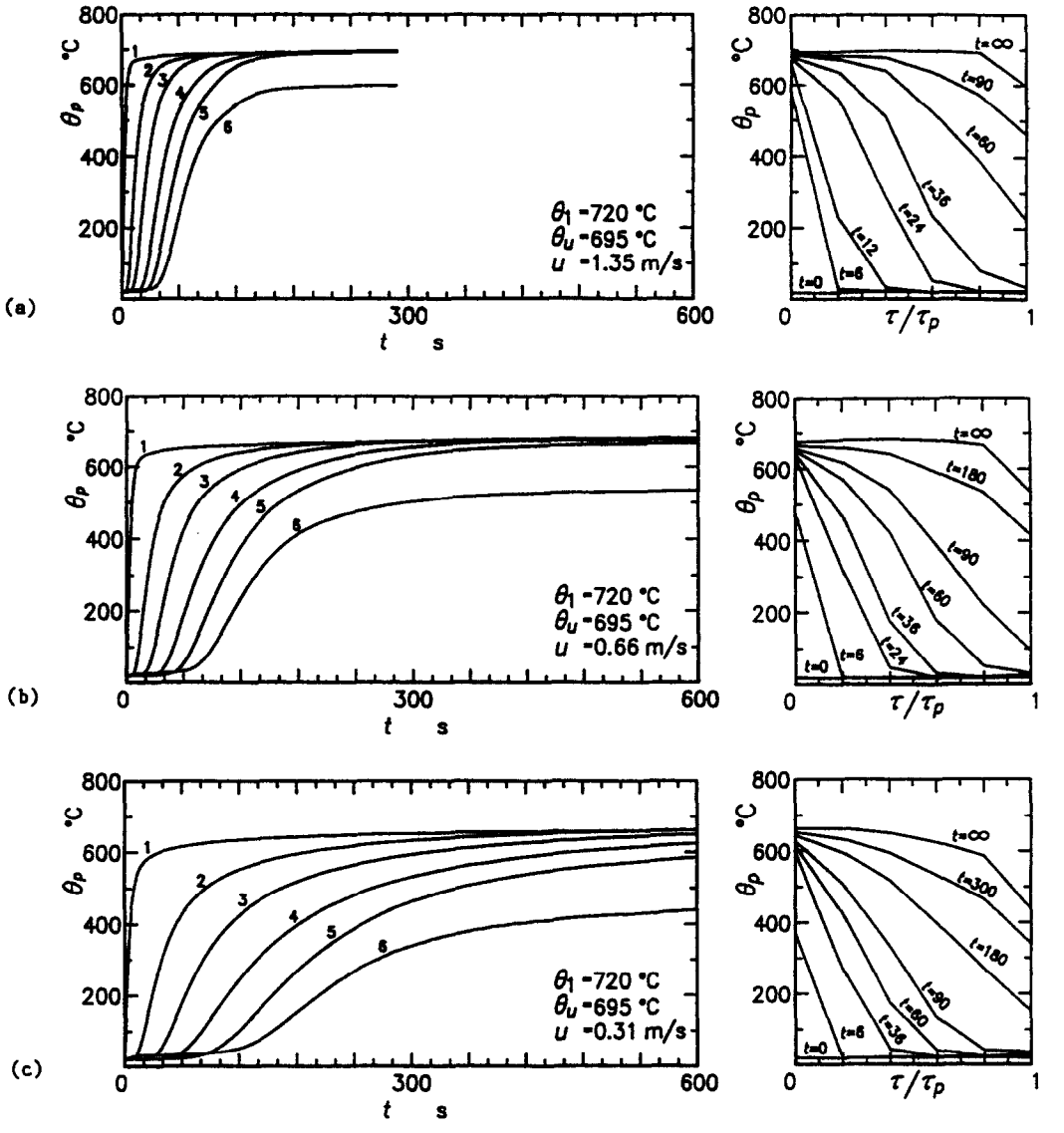

FIG. 5. Measured temperature variations: (a) $u = 1.35$ m s^{-1}; (b) $u = 0.66$ m s^{-1}; (c) $u = 0.31$ m s^{-1}.

lowest gas velocity (Fig. 5(c)). Owing to such a quick response, the system exhibits high potentiality as a radiative converter for use in industry.

4.2. *Comparison of predictions with experimental data*

Figures 6(a)–(c) compare the predicted and measured temperatures for three sets of Θ_u and *Pe*. Subsidiarily, the results of the cooling process are compared in Fig. 7. In each line pair, the dotted line is the dimensionless gas temperature Θ_g, while the solid line the dimensionless porous medium temperature Θ_p. The open symbols denote the measured data of Θ_p. The agreement between the analysis and experiment is satisfactory. Thus, we conclude that the assumptions and numerical scheme used in the analysis are valid.

4.3. *Discussion based on the predicted results*

Since the prediction proved to be accurate enough, we discuss the heat transfer characteristics of the system on the basis of the predicted results. Before examining the effect of various parameters, we point out some features which are common to all cases shown in Fig. 6.

(1) The calculated temperatures Θ_g and Θ_p are very close to each other. This is because the heat transfer between the gas and porous media is very efficient owing to the small characteristic length and large heat transfer area.

(2) For an initial period, the exit gas temperature (Θ_g at $X = 1$) does not increase from that of the room temperature, Θ_0. In this period, the available energy of the working gas is perfectly transferred to the

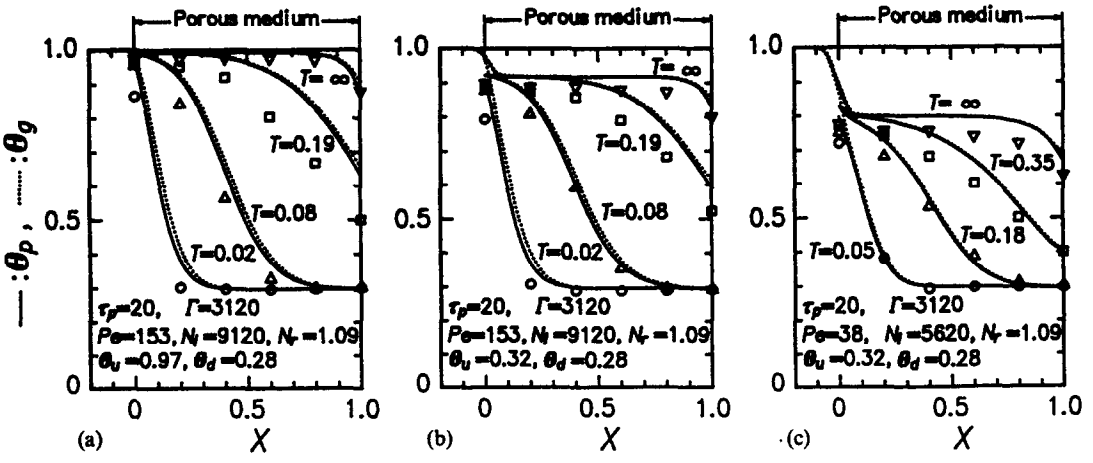

FIG. 6. Comparison of measured and predicted temperatures: (a) $Pe = 153$ ($N_t = 9120$), $\Theta_u = 0.97$; (b) $Pe = 153$ ($N_t = 9120$), $\Theta_u = 0.32$; (c) $Pe = 38$ ($N_t = 5620$), $\Theta_u = 0.32$.

porous medium, and the radiative heat transfer to the downstream direction is negligible. Hence, the present radiative converter serves also as a thermal insulator during this period. The duration is an important factor when designing unsteadily operated equipment with a porous medium.

Comparison between Figs. 6(a) and (b) shows the effect of incident radiation from the upstream side (the effect of Θ_u). The porous medium temperature Θ_p decreases with decreasing Θ_u. As shown later, this is ascribed to the increase of thermal energy transferred to the upstream direction from the porous medium.

The effect of the Peclet number Pe is shown by comparing Figs. 6(b) and (c). It is evident that for a small Peclet number the gas temperature sharply drops at the region immediately upstream of the porous medium. The temperature drop is caused by heat conduction to the downstream region where the gas is cooled by the porous medium.

The energy transport in the system can be readily understood in terms of the radiative heat flux. First, its steady-state distributions are shown in Figs. 8(a)–(c), corresponding to Figs. 6(a)–(c), respectively. As is clearly seen in the figures, the absolute value of the net radiative heat flux $|Q_n|$ is zero in the majority of the porous medium, but increases sharply near the entrance and exit of the porous medium. One of the most important quantities of the radiative converter is the net radiative heat flux at the entrance of the porous medium $\tau = 0$. Hence, in the following, attention is focused chiefly on it. In Fig. 8(b) where $\Theta_u < \Theta_1$, the net radiative heat flux has a large negative value, which means that the energy is transferred to the upstream direction; such a directional transport ($Q_n < 0$) is essential for the radiative converter. On the other hand, in Fig. 8(a) where $\Theta_u \simeq \Theta_1 = 1$, the net radiative heat flux Q_n at $\tau = 0$ is about zero; this radiation shield ($Q_n \simeq 0$) is attained by large Q^- ($\simeq R_u$), and is also useful for practical applications.

Figures 9(a)–(c) show the transient behavior of the radiative heat flux. Solid lines denote Q_n, Q^+, and Q^- at the entrance of the porous medium, while dotted lines denote Q_n at the exit. At $X = 0$, even in case (c) of the relatively low Peclet number, Q_n reaches the steady value for $T \simeq 0.1$, which corresponds to about 50 s in an actual operating condition. At $X = X_p$, however, the time constant for Q_n is about one order of magnitude larger than that at $X = 0$. The period when Q_n at $X = X_p$ remains zero corresponds to that when the exit gas temperature (Θ_g at $X = 1$) does not increase from the room temperature Θ_0.

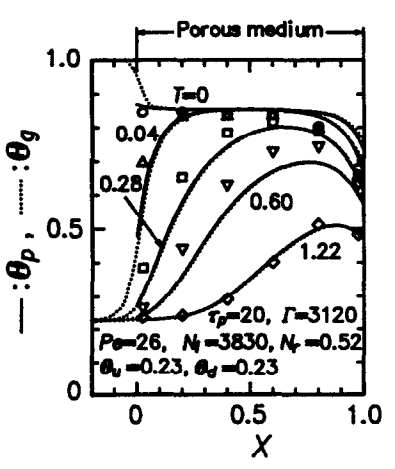

FIG. 7. Comparison of measured and predicted temperatures in the cooling experiment.

5. CONCLUSIONS

The transient characteristics of combined conduction, convection and radiation heat transfer in the porous medium were analyzed assuming the porous medium to be a homogeneous continuum. To assess the accuracy of the predictions, experiments which corresponded strictly to the analyzed system were

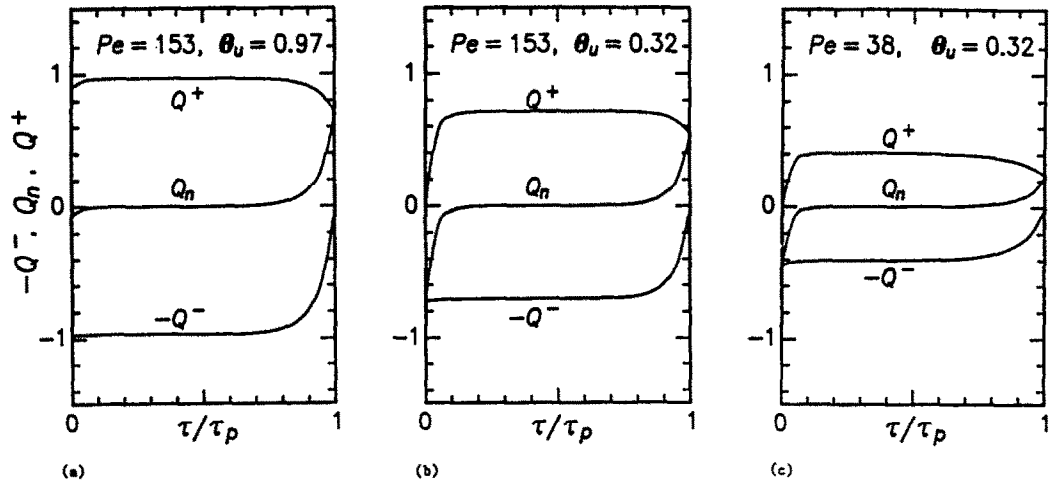

FIG. 8. Distributions of radiative heat flux for three steady-state conditions: (a) $Pe = 153$ ($N_l = 9120$), $\Theta_u = 0.97$; (b) $Pe = 153$ ($N_l = 9120$), $\Theta_u = 0.32$; (c) $Pe = 38$ ($N_l = 5620$), $\Theta_u = 0.32$.

performed. The predictions were found to agree satisfactorily with the experimental data. The significant improvement of the predicted results compared with those of the previous paper is ascribed to take into account the gas-phase heat conduction.

The principal results concerning the thermal response of the radiative converter are summarized as follows.

(1) The time constant of the whole system increases

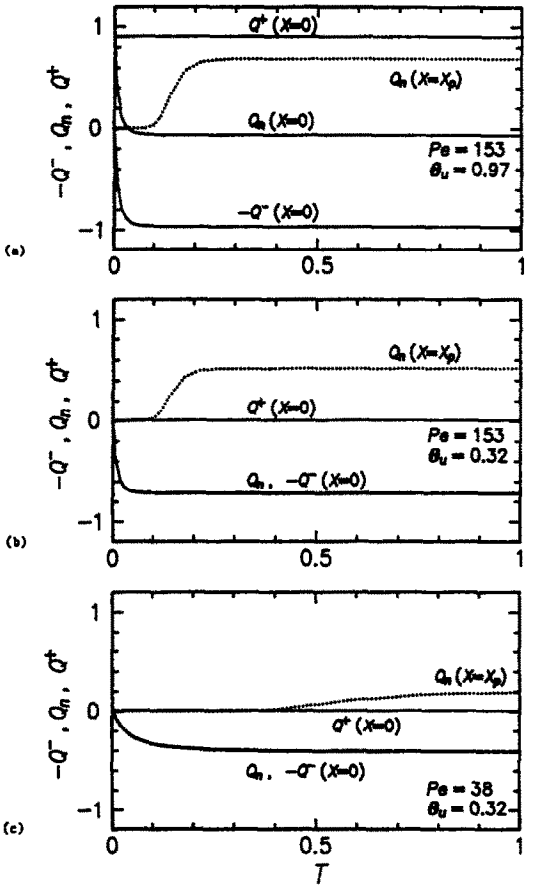

FIG. 9. Transient behavior of radiative heat flux at the entrance of the porous medium: (a) $Pe = 153$ ($N_l = 9120$), $\Theta_u = 0.97$; (b) $Pe = 153$ ($N_l = 9120$), $\Theta_u = 0.32$; (c) $Pe = 38$ ($N_l = 5620$), $\Theta_u = 0.32$.

with decreasing gas velocity; in practical working conditions, it is of the order of 100 s. The local time constant, however, varies largely in the porous medium. The response at the entrance of the porous medium is much quicker than that at the exit.

(2) As a result, the net radiative heat flux at the entrance of the porous medium, which is one of the most important quantities for the radiative converter, rapidly reaches the steady value (usually within 50 s).

(3) The relatively slow response at the exit of the porous medium is also significant, especially for periodically operated equipment.

Acknowledgement—The authors would like to thank N. Masuda, T. Sato, K. Suzuki, and G. Nagahara, former students at the Department of Mechanical Engineering, Tokyo Institute of Technology, for their assistance in carrying out the experimental studies. The authors wish to express their appreciation to Tokyo Gas Co., Ltd. for manufacturing and supplying the high-performance heat exchanger. This work was supported in part by the Ministry of Education, Science and Culture under a Grant-in-Aid for Scientific Research Type A, No. 60420028.

REFERENCES

1. R. Echigo, Effective energy conversion method between gas enthalpy and thermal radiation and application to industrial furnaces, *Proc. 7th Int. Heat Transfer Conf.*, München, Vol. 6, pp. 361–366 (1982).
2. R. Echigo, M. Kurusu, K. Ichimiya and Y. Yoshizawa, Combustion augmentation of extremely low calorific gases (application of the effective energy conversion method from gas enthalpy to thermal radiation), *Proc. 1983 ASME–JSME Thermal Engng Joint Conf.*, Honolulu, Vol. IV, pp. 99–103 (1983).
3. R. Echigo, High temperature heat transfer augmentation. In *High Temperature Heat Exchangers* (Edited by Y. Mori, A. E. Sheindlin and N. Afgan), pp. 230–259. Hemisphere, Washington, DC (1986).
4. R. Echigo, Sophisticated applications of radiation heat transfer. In *Heat Transfer in High Technology and Power Engineering* (Edited by W.-J. Yang and Y. Mori), pp. 503–514. Hemisphere, Washington, DC (1987).
5. Y. Yoshizawa, R. Echigo and T. Tomimura, A study on a high performance radiant heater, *Proc. 1987 ASME–JSME Thermal Engng Joint Conf.*, Honolulu, Vol. 5, pp. 317–323 (1987).
6. R. Echigo, K. Hanamura, Y. Yoshizawa and T. Tomimura, Radiative heat transfer enhancement to a water tube by combustion gases in porous media. In *Heat Transfer Science and Technology* (Edited by B.-X. Wang), pp. 703–710. Hemisphere, Washington, DC (1987).
7. Y. Yoshizawa, K. Sasaki and R. Echigo, Analytical study of the structure of radiation controlled flame, *Int. J. Heat Mass Transfer* **31**, 311–319 (1988).
8. R. Echigo, H. Yoshida and T. Mochizuki, Temperature equalization by the radiative converter for a slab in continuous casting direct rolling, *JSME Int. J. Ser. II* 31(3), 545–552 (1988).
9. K. Y. Wang and C. L. Tien, Thermal insulation in flow systems: combined radiation and convection through a porous segment, *J. Heat Transfer* **106**, 453–459 (1984).
10. R. Echigo, T. Tomimura, Y. Yoshizawa and H. Jinnouchi, Effective energy conversion method between gas enthalpy and thermal radiation (effects of gaseous radiation and incoming radiations), *Rep. Inst. Adv. Mater. Study, Kyusyu Univ.* 2(1), 53–66 (1988).
11. J. D. Knudsen and D. L. Katz, *Fluid Dynamics and Heat Transfer*, pp. 504–505. McGraw-Hill, New York (1958).

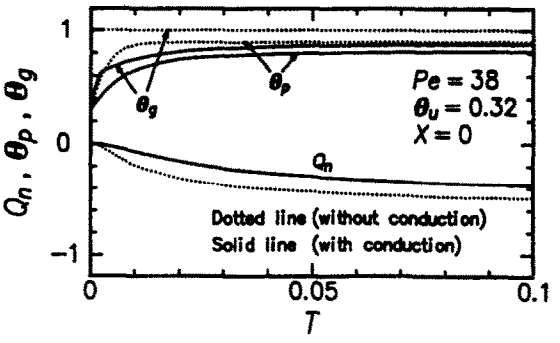

FIG. A1. Initial response at the entrance of the porous medium with and without gas-phase conduction.

APPENDIX A

The effect of gas-phase conduction is discussed in the following. Figure A1 shows the initial response at the entrance of the porous medium for the case of relatively low Peclet number. The solid and dotted lines denote the results with and without the gas-phase conduction, respectively. The most essential difference is seen in the variations of the gas temperature Θ_g. In the case without conduction, Θ_g is constant and equal to unity because it is fixed by the boundary condition. In the case with conduction, however, Θ_g gradually increases and asymptotically reaches 0.88. As a result, the calculated response for the case without conduction is much quicker than that with conduction (or the real case).

The temperature distributions for the steady-state condition are compared in Fig. A2. Although there is con-

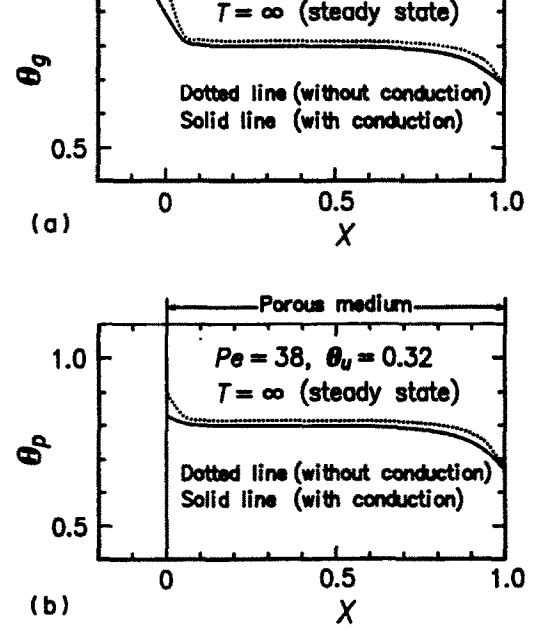

FIG. A2. Steady-state temperature distributions with and without gas-phase conduction: (a) gas temperature; (b) porous-medium temperature.

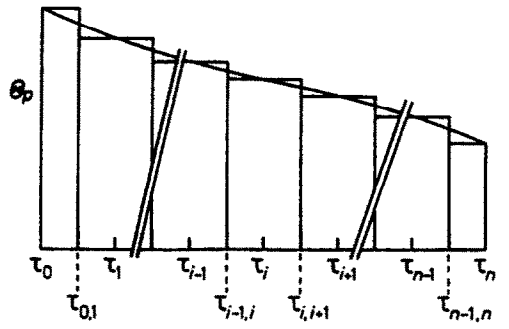

FIG. B1. Numerical integration using the trapezoidal rule.

siderable difference near the upstream end of the porous medium, the overall distributions do not differ much from each other. Hence, we conclude the gas-phase conduction becomes important for the initial period with low Peclet number.

APPENDIX B

A complete derivation of equations (19)–(21) is presented here. As shown in Fig. B1, the trapezoidal rule is used to numerically integrate the radiative heat flux and its divergence. Using the arrays of variables listed in Table B1, they are approximated as follows:

equation (19)

$$\begin{aligned}
&\int_0^{\tau_i}\Theta_p(\tau')^4E_2(\tau_i-\tau')\,d\tau' \\
&\quad=\Theta_p(\tau_0)^4\int_{\tau_0}^{\tau_{0,1}}E_2(\tau_i-\tau')\,d\tau' \\
&\qquad+\sum_{j=1}^{i-1}\left(\Theta_p(\tau_j)^4\int_{\tau_{j-1,j}}^{\tau_{j,j+1}}E_2(\tau_i-\tau')\,d\tau'\right) \\
&\qquad+\Theta_p(\tau_i)^4\int_{\tau_{i-1,i}}^{\tau_i}E_2(\tau_i-\tau')\,d\tau' \\
&\quad=\Theta_p(\tau_0)^4[E_3(\tau_i-\tau_{0,1})-E_3(\tau_i-\tau_0)] \\
&\qquad+\sum_{j=1}^{i-1}(\Theta_p(\tau_j)^4[E_3(\tau_i-\tau_{j,j+1})-E_3(\tau_i-\tau_{j-1,j})]) \\
&\qquad+\Theta_p(\tau_i)^4[E_3(\tau_i-\tau_i)-E_3(\tau_i-\tau_{i-1,i})] \\
&\quad=\sum_{j=0}^{i-1}\Theta_p(\tau_j)^4[E_3(\mathrm{DTIJ1}(i,j))-E_3(\mathrm{DTIJ}(i,j))] \\
&\qquad+\Theta_p(\tau_i)^4[E_3(0)-E_3(\mathrm{DTIJ}(i,i))] \\
&\quad=\sum_{j=0}^{i}[\Theta_{pj}^4\mathrm{E3MATP}(i,j)]; \qquad \text{(B1)}
\end{aligned}$$

equation (20)

$$\begin{aligned}
&\int_{\tau_i}^{\tau_p}\Theta_p(\tau')^4E_2(\tau'-\tau_i)\,d\tau' \\
&\quad=\Theta_p(\tau_i)^4\int_{\tau_i}^{\tau_{i,i+1}}E_2(\tau'-\tau_i)\,d\tau' \\
&\qquad+\sum_{j=i+1}^{n-1}\left(\Theta_p(\tau_j)^4\int_{\tau_{j-1,j}}^{\tau_{j,j+1}}E_2(\tau'-\tau_i)\,d\tau'\right) \\
&\qquad+\Theta_p(\tau_n)^4\int_{\tau_{n-1,n}}^{\tau_n}E_2(\tau'-\tau_i)\,d\tau' \\
&\quad=-\Theta_p(\tau_i)^4[E_3(\tau_{i,i+1}-\tau_i)-E_3(\tau_i-\tau_i)] \\
&\qquad-\sum_{j=i+1}^{n-1}(\Theta_p(\tau_j)^4[E_3(\tau_{j,j+1}-\tau_i) \\
&\qquad-E_3(\tau_{j-1,j}-\tau_i)]) \\
&\qquad-\Theta_p(\tau_n)^4[E_3(\tau_n-\tau_i)-E_3(\tau_{n-1,n}-\tau_i)] \\
&\quad=-\Theta_p(\tau_i)^4[E_3(-\mathrm{DTIJ1}(i,i))-E_3(0)] \\
&\qquad-\sum_{j=i+1}^{n}\Theta_p(\tau_j)^4[E_3(-\mathrm{DTIJ1}(i,j)) \\
&\qquad-E_3(-\mathrm{DTIJ}(i,j))] \\
&\quad=\sum_{j=i}^{n}[\Theta_{pj}^4\mathrm{E3MATN}(i,j)]; \qquad \text{(B2)}
\end{aligned}$$

equation (21)

$$\begin{aligned}
&2\Theta_p(\tau_i)^4-\int_0^{\tau}\Theta_p(\tau')^4E_1(\tau-\tau')\,d\tau' \\
&\qquad-\int_{\tau}^{\tau_p}\Theta_p(\tau')^4E_1(\tau'-\tau)\,d\tau' \\
&\quad=2\Theta_p(\tau_i)^4-\Theta_p(\tau_0)^4\int_{\tau_0}^{\tau_{0,1}}E_1(\tau_i-\tau')\,d\tau' \\
&\qquad-\sum_{j=1}^{i-1}\left(\Theta_p(\tau_j)^4\int_{\tau_{j-1,j}}^{\tau_{j,j+1}}E_1(\tau_i-\tau')\,d\tau'\right) \\
&\qquad-\Theta_p(\tau_i)^4\int_{\tau_{i-1,i}}^{\tau_i}E_1(\tau_i-\tau')\,d\tau' \\
&\qquad-\Theta_p(\tau_i)^4\int_{\tau_i}^{\tau_{i,i+1}}E_1(\tau'-\tau_i)\,d\tau' \\
&\qquad-\sum_{j=i+1}^{n-1}\left(\Theta_p(\tau_j)^4\int_{\tau_{j-1,j}}^{\tau_{j,j+1}}E_1(\tau'-\tau_i)\,d\tau'\right) \\
&\qquad-\Theta_p(\tau_n)^4\int_{\tau_{n-1,n}}^{\tau_n}E_1(\tau'-\tau_i)\,d\tau' \\
&\quad=2\Theta_p(\tau_i)^4-\Theta_p(\tau_0)^4[E_2(\tau_i-\tau_{0,1})-E_2(\tau_i-\tau_0)]
\end{aligned}$$

Table B1. Arrays of new variables introduced in equations (B1)–(B3)

Variables	Arrays
τ_i	→ TAU(i)
$\tau_{i,i+1}=(\tau_i+\tau_{i+1})/2$	→ TAU1(i) = (TAU(i)+TAU($i+1$))/2
$\tau_{-1,0}=\tau_0$	→ TAU1(-1) = TAU(0)
$\tau_{n,n+1}=\tau_n$	→ TAU1(n) = TAU(n)
$\tau_i-\tau_{j-1,j}$	→ DTIJ(i,j) = TAU(i)−TAU1($j-1$)
$\tau_i-\tau_{j,j+1}$	→ DTIJ1(i,j) = TAU(i)−TAU1(j)

$$
\begin{aligned}
&-\sum_{j=1}^{i-1}(\Theta_p(\tau_j)^4[E_2(\tau_i-\tau_{j,j+1})-E_2(\tau_i-\tau_{j-1,j})])\\
&-\Theta_p(\tau_i)^4[E_2(\tau_i-\tau_i)-E_2(\tau_i-\tau_{i-1,i})]\\
&+\Theta_p(\tau_i)^4[E_2(\tau_{i,i+1}-\tau_i)-E_2(\tau_i-\tau_i)]\\
&+\sum_{j=i+1}^{n-1}(\Theta_p(\tau_j)^4[E_2(\tau_{j,j+1}-\tau_i)-E_2(\tau_{j-1,j}-\tau_i)])\\
&+\Theta_p(\tau_n)^4[E_2(\tau_n-\tau_i)-E_2(\tau_{n-1,n}-\tau_i)]
\end{aligned}
$$

$$
\begin{aligned}
&=\sum_{j=0}^{i-1}(\Theta_p(\tau_j)^4[E_2(\mathrm{DTIJ}(i,j))-E_2(\mathrm{DTIJ1}(i,j)])\\
&+\Theta_p(\tau_i)^4 2E_2(\mathrm{DTIJ}(i,i))\\
&+\sum_{j=i+1}^{n}(\Theta_p(\tau_j)^4[E_2(-\mathrm{DTIJ1}(i,j))\\
&-E_2(-\mathrm{DTIJ}(i,j))])\\
&=\sum_{j=0}^{n}[\Theta_{pj}^4\mathrm{E2MAT}(i,j)]. \qquad \text{(B3)}
\end{aligned}
$$

CARACTERISTIQUES VARIABLES DU TRANSFERT THERMIQUE COUPLE PAR CONDUCTION, CONVECTION ET RAYONNEMENT DANS LES MILIEUX POREUX

Résumé—On présente les caractéristiques variables de transfert thermique d'une convection effective d'énergie entre l'enthalpie du gaz à haute température et le rayonnement à l'aide du milieu poreux. Une analyse théorique est conduite pour un système monodimensionnel siège de conduction, convection et rayonnement. On suppose que le milieu poreux est homogène et qu'il absorbe et émet le rayonnement. Les équations d'énergie couplées pour le gaz et le milieu poreux sont résolues numériquement. Pour confirmer la validité de l'analyse, des expériences sont conduites dans le conditions correspondant au modèle analytique. Les résultats du calcul s'accordent bien avec ceux de l'expérience.

DAS INSTATIONÄRE VERHALTEN DES WÄRMEÜBERGANGS DURCH WÄRMELEITUNG, KONVEKTION UND STRAHLUNG IN EINEM PORÖSEN MEDIUM

Zusammenfassung—In dieser Arbeit wird über das instationäre Verhalten des Wärmeübergangs von einem Gas hoher Temperatur an ein poröses Medium berichtet. Ein eindimensionales System wird theoretisch untersucht, in dem gleichzeitig Wärmeleitung, Konvektion und Strahlung stattfinden. Das poröse Medium wird als homogenes Kontinuum angesehen, das Wärmestrahlung absorbiert und emittiert. Die gekoppelten Energiegleichungen für das Gas und das poröse Medium werden numerisch gelöst. Die Rechenergebnisse werden mit entsprechenden Versuchsdaten verglichen, wobei sich gute Übereinstimmung zeigt.

ПЕРЕХОДНЫЕ ХАРАКТЕРИСТИКИ КОМБИНИРОВАННОГО КОНДУКТИВНОГО, КОНВЕКТИВНОГО И РАДИАЦИОННОГО ТЕПЛОПЕРЕНОСА В ПОРИСТЫХ СРЕДАХ

Аннотация—Представлены переходные характеристики теплопереноса при эффективном энергообмене между энтальпией высокотемпературного газа и тепловым излучением в пористых средах. Проводится теоретический анализ одномерных систем, в которых одновременно присутствуют процессы теплопроводности, конвекции и излучения. Предполагается, что пористая среда представляет собой однородный континуум, поглощающий и испускающий тепловое излучение. Численно решаются сопряженные уравнения сохранения энергии для газа и пористых сред. Для подтверждения справедливости данного анализа проведены эксперименты в строгом соответствии с аналитической моделью. Расчетные результаты хорошо согласуются с экспериментальными данными.